

Development of Micromachine Gas Turbines at Tohoku University

Kousuke Isomura

Ishikawajima-Harima Heavy Industries Co., Ltd.
3-5-1 Mukodai-cho Nishi-Tokyo-shi
Tokyo 188-8555
JAPAN

Kousuke_isomura@ihi.co.jp

Shuji Tanaka

Tohoku University, Aza-Aoba 01
Aramaki Aoba-ku, Sendai-shi 980-8579
JAPAN

Shin-ichi Togo

Tohoku-Gakuin University
13-1 Chuo 1-chome, Tagajo-shi 985-8537
JAPAN

Hideki Kanebako

Sankyo Seiki Mfg. Co., Ltd.
5329 Shimosuwa-machi, Suwa-gun
Nagano 393-8511
JAPAN

ACKNOWLEDGEMENT

The basic research on high-speed gas bearings has been supported by The Asian Office of Aerospace Research and Development (AOARD), grant number F62562-03-T-0452, program manager Dr. Brett Pokines. The development of high-speed turbomachinery was supported by The New Energy and Industrial Technology Development Organization of Japan (NEDO).

ABSTRACT

Development of micromachine gas turbines is underway at a group lead by Tohoku University in Japan. The goal is to develop a light-weight power source to replace the heavy batteries that may limit the progress of humanoid robots. Internal combustion engines have advantages of both high power density and high energy density, so it can be the best choice for the power source for mobile machines. The project is currently challenging to develop the smallest possible gas turbine of three-dimensional geometry to be fabricated by machining. The micro-combustor has already been completed the validation test, and experimental validation of the turbo-unit and the generator of the diameter 10mm is underway. Current major technical challenges are the development of the bearings to sustain the high-speed rotation of the rotors and the technologies to fabricate the bearings within the required tolerance.

1.0 INTRODUCTION

1.1 New Market for Portable Power Generation

One of the technologies that is rapidly progressing to the level of practical use these days, is a humanoid robot. There are number of projects all over the world, from national team level to private company level, to develop variety of humanoid robots. Especially after Honda's humanoid robot Asimo (Figure 1-1) debuted to the world, people realized the vast capability of humanoid robots, and research and development of robot has now become a boom.

Isomura, K.; Tanaka, S.; Togo, S.-I.; Kanebako, H. (2005) Development of Micromachine Gas Turbines at Tohoku University. In *Micro Gas Turbines* (pp. 10-1 – 10-34). Educational Notes RTO-EN-AVT-131, Paper 10. Neuilly-sur-Seine, France: RTO. Available from: <http://www.rto.nato.int/abstracts.asp>.



Figure 1-1: Asimo of Honda.

(from Asimo home page; <http://www.honda.co.jp/ASIMO/>)

When many people start the research and the technology level increases, the system becomes more and more complicated and sophisticated, and hence, variety of applications and concepts appear. Toyota has recently revealed several types of their new robots that have different function from Asimo. They have a capability of playing trumpet with their controllable soft lip with a breath (Figure 1-2). National Institute of Advanced Industrial Science and Technology (AIST) and The University of Tokyo jointly succeeded in let HRP-2 robot to dance the traditional Japanese folk dance “Aizu Bandaisan” by simulating the dance master’s movement (Figure 1-3). This technology requires collateral movement of many servomotors at various joints at the same time. Hence, the power requirements for the advanced robots are increasing.



Figure 1-2: Toyota’s Robots to Play Trumpet.

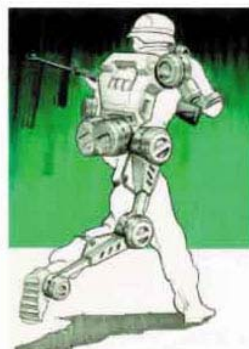
(from Toyota’s home page; <http://www.toyota.co.jp/jp/special/robot/index.html>)



Figure 1-3: HRP-2 of AIST Dancing “Aizu Bandaisan” with a Dance Master.
http://www.aist.go.jp/aist_j/press_release/pr2005/pr20050112/pr20050112.html

Other than the autonomous humanoid robots, powered mechanisms to aid human motion are also under development. Figure 1-4 shows the DARPA’s concept sketch of future armour called exoskeleton that increases the loading and running capability of soldiers. Prototype of such machine is developed at U.C. Berkeley is called Berkeley Lower Extremity Exoskeleton (BLEEX), and is shown in Figure 1-5. The backpack of the man wearing the BLEEX is explained to be capable of carrying 120 pounds of loads, but it is easy to imagine that the power source to drive such a device long enough for the practical mission may weigh about the whole loading capacity. Figure 1-6 shows the people mover that Toyota is currently developing. It carries the whole weight of a man, so the power requirement would be even larger.

 Exoskeleton Applications - Examples



Enhanced speed and mobility



Armored Soldier

Figure 1-4: DARPA’s Conceptual Sketch of Exoskeleton.
<http://www.darpa.mil/dso>



Figure 1-5: U.C. Berkeley's BLEEX.

(http://www.berkeley.edu/news/media/releases/2004/03/03_exo.shtml)



Figure 1-6: Toyota's People Mover.

(<http://www.toyota.co.jp/jp/special/robot/index.html>)

All of these machines are using batteries such as Nickel-Metal Hydride batteries and Lithium-ion batteries, for the power sources. Hence, the weight of the power source is very heavy, and the operational time is very limited. Asimo, which requires only 380W, can operate only 30 minutes after half a day of

recharging. The more complex robots' operating time is even shorter. The reason for those robots using only batteries is simply that the number one technical issues to realize robots have been sophisticated control of the movement synchronized with related sensing and image processing. Almost all the researchers developing robots are in such fields, which is very different from the field of power generation, so they might have stuck to the existing reliable power source to reduce the technical challenges. It has already been very challenging to develop the autonomous walking robots. When the control technology is matured and the development comes to the phase of practical system in near future, they will certainly start looking for a better power source. One of such movement can be seen as the Palm Power initiative by DARPA that started in year 2001. The Palm Power initiative is a technology development program that will advance the technology as far as possible by demonstrating new approaches that will ultimately lead to complete system demonstrations. The requirement of the target systems shown in the Palm Power initiative is shown in Figure 1-17. The figure shows that the required energy densities are far beyond those available by batteries, and therefore a technology development program has been started. In the same year a study on micro-power sources has been conducted [1].

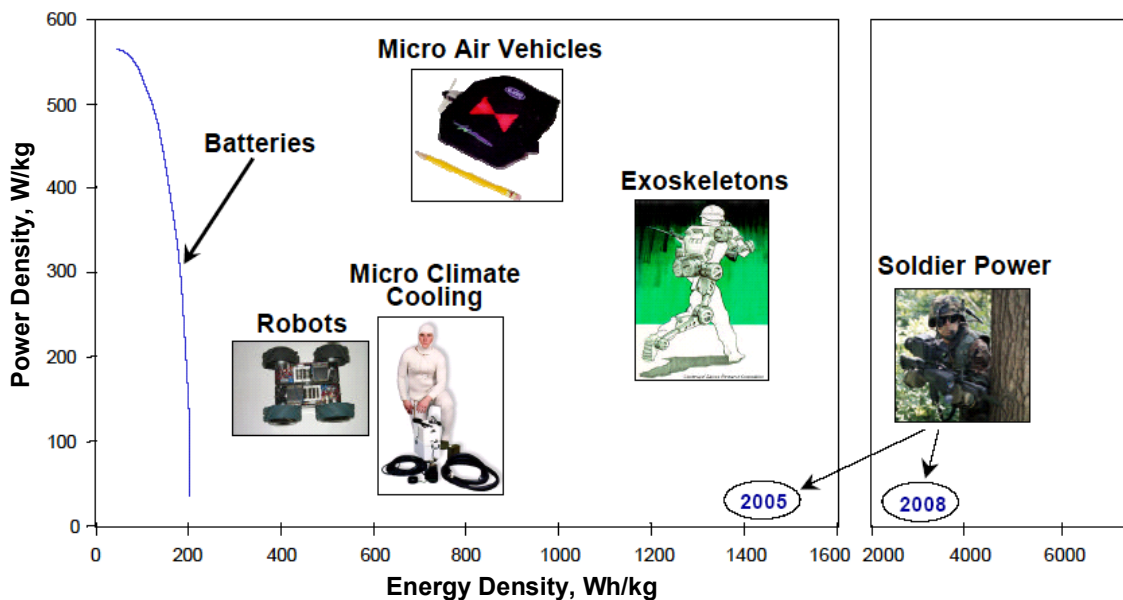


Figure 1-7: Variety of Mobile Power Requirements shown in DARPA Palm Power Project.

(<http://www.darpa.mil/dso/thrust/matdev/palmpower>)

Many people think fuel cells are the most promising power sources in future. However, not only that the development of fuel cell will take more time, but also, fuel cell is very heavy, and therefore, it is not a power source suitable for mobile machine as robots. The power character of various power sources is shown in Figure 1-8. The power density is the power (watt = voltage x current) divided by system weight, and the energy density (watt hour = watt x operation time before recharging) divided by system weight. Fuel cells have large energy density, but have low power density, while the character required for power sources for mobile machines is large power density. Note that the applications shown in Figure 1-7 require the power density higher than 200W/kg, while that of fuel cells shown in Figure 1-8 is an order smaller 20W/kg, at most. The efficiency of the fuel cell drops when the current density in the cell stack becomes large. This means that fuel cells need to be large to reduce the current density, or the application should not require large current, but require large voltage, to achieve high efficiency. Hence, fuel cells are good for driving IC based electronic equipments, but not good at driving electric motors in mobile machines that the weight of the system will penalize the performance.

From Figure 1-8, the power sources capable of providing large power density are internal combustion engines and batteries. Since batteries have very low energy density, they cannot provide long operation time. Therefore, the best power source to solve the short duration time problem of batteries will be the internal combustion engines. Note that Hydrocarbon fuel commonly used for internal combustion engines, such as JP-8, contains 13,200 Wh of energy per kg. Hence power generations from hydrocarbon fuel have capability of further increasing the energy density to an order larger value by technology innovations and by combination and integration of multiple of generation methods into a system.

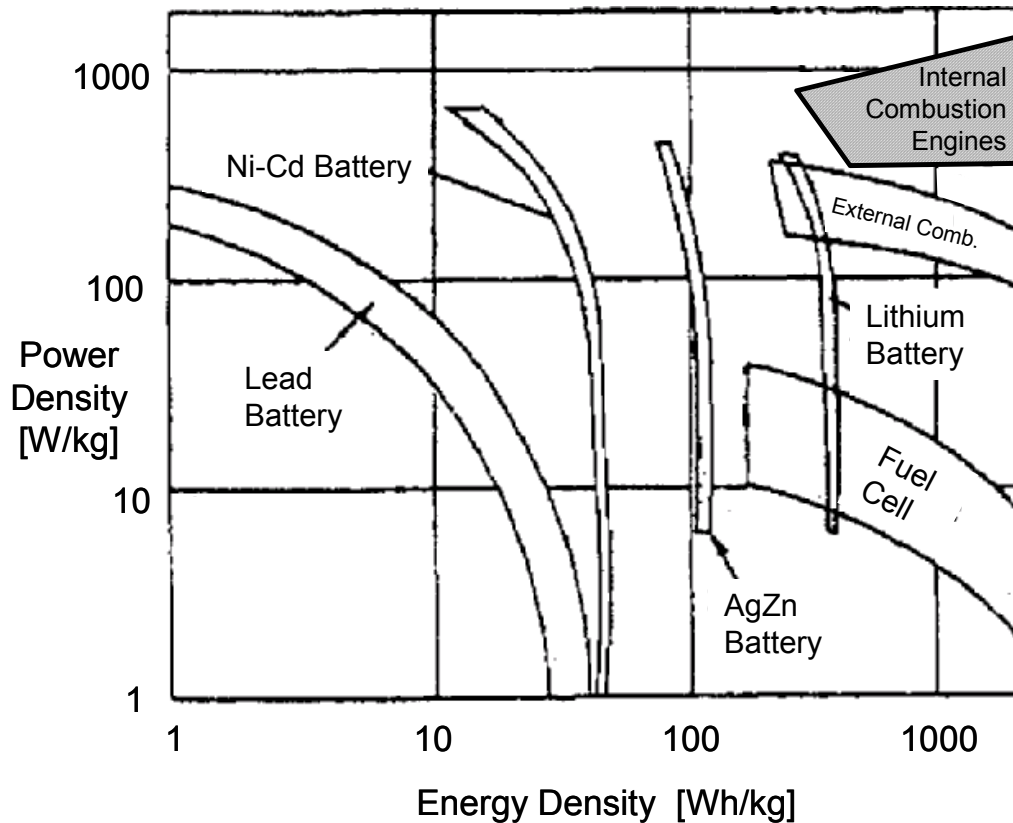


Figure 1-8: Power Density and Energy Density of Various Power Sources. [1]

To select the configuration of the base system, there is a wide variety of internal combustion engines to choose from. Although the power requirement of the robots is increasing, it is still very small for the current size of internal combustion engines. Therefore, the internal combustion engines to power the robots have to be miniaturized. The major obstacles for miniaturizing the internal combustion engines are, (1) heat isolation, and (2) friction reduction. One important parameter to affect the efficiency of the internal combustion engine is the temperature difference between the maximum temperature and the minimum temperature in the cycle. Usually, the minimum temperature is the ambient temperature, and the maximum temperature is the combustion temperature. Since it is difficult to maintain high temperature in intermittent combustion, it would be better select the cycles that use continuous combustion. For the friction problem, reciprocating engines are generally known for their large friction characters. Rotary engines will also suffer from the friction at the apex seals. Therefore, the engine cycle with continuous rotation is preferable.

The engine cycles to satisfy both continuous combustion and continuous rotation requirements are gas turbine and steam turbine. Since the steam turbine system is very complex, gas turbine cycle is selected as the cycle for the base system to be developed.

2.2 Compressor

The rotor speed of gas turbine is defined by the required pressure ratio of the compressor. The required compressor pressure ratio is found from the cycle study. In the cycle of 100W micromachine gas turbine shown in Figure 2-1, the compressor is required to generate pressure ratio 3. From the pressure ratio, the required impeller tip tangential speed is calculated to be about 450m/sec. Since the tangential speed is a product of the rotational speed and the impeller diameter, the rotational speed becomes inversely proportional to the rotor diameter. Hence, the shaft speed increases as the impeller diameter reduces. This relation for pressure ratio 3 is shown in Figure 2-3. For current impeller of diameter 10mm, the required shaft speed is found to be 870,000 rpm. Hence, the requirement for the compressor is to run stably at 870,000 rpm, and generate pressure ratio 3 at 68% of the adiabatic efficiency.

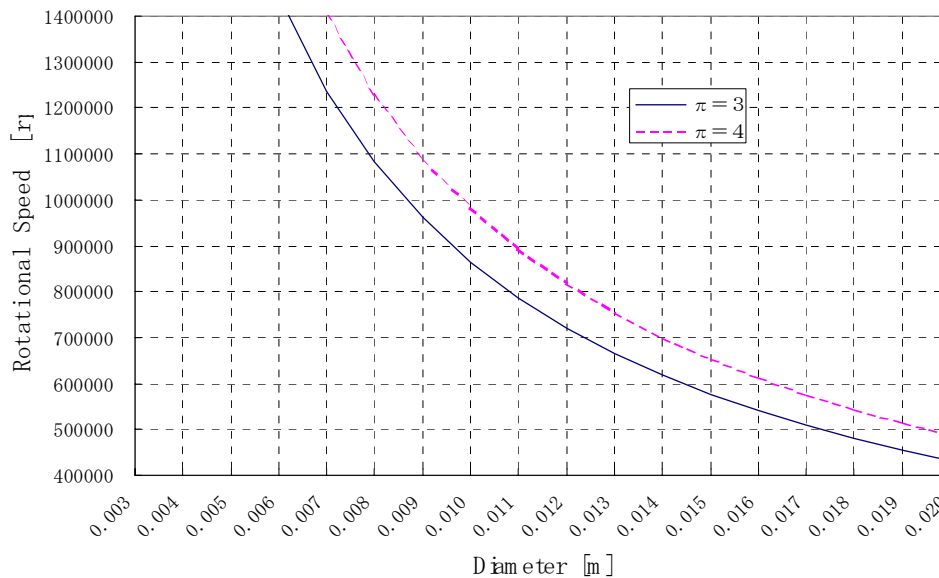


Figure 2-3: Rotor Diameter and Shaft Speed for a Compressor with Pressure Ratio 3.

There are two major technical challenges in these requirements. The first challenge is the very high rotor speed. The common measure of the performance of ball bearings is a DN number, which is a product of diameter D in mm, and shaft speed N in rpm. If we use a shaft of diameter 4mm to support this rotor, which looks to be about the smallest limit to support 10mm diameter impellers, the DN number becomes 3,480,000. This number is beyond that of currently available bearings for practical use. This DN number is about the champion data in laboratory environment of bearing test rig with excessive amount of lubrication oil. For the practical use, DN number around 2,000,000 would be a reasonable limit, if long life is required. For 4mm shaft, it is 500,000 rpm. If we limit the selection of bearing as ball bearings, which are the most matured and reliable bearing of these days, we have to reduce the shaft speed. The reduction of the shaft speed will require the increase of the impeller diameter to achieve the same pressure ratio. Since the centrifugal compressor impellers have the range of exit blade height to diameter ratio to operate at reasonable adiabatic efficiency (Figure 2-4), the efficiency will be penalized to keep the same output power when the impeller diameter increases. If we keep the exit blade height to diameter ratio about the same, it will result in the increase of the mass flow rate, and hence in the increase of the output power. Therefore, a very high shaft speed is required, and high speed bearings are essential for realizing very small gas turbines. An alternative to the ball bearings has to be developed for the shaft speed over 500,000 rpm, of which the speed has not realized in gas turbines, before.

There is another difficulty in realizing the required compressor efficiency for micromachine gas turbines. That is the heat conduction into the compressor from the combustor and the turbine. When heat is added, the density of the flow reduces and the compressor impeller cannot add the designed work to the flow. Hence the adiabatic efficiency of the compressor drops. Figure 2-6 shows the extent of the efficiency drop assessed by CFD calculation with isothermal wall boundary conditions. The effect of heat addition is remarkable that the compressor efficiency drops as large as 10% by increasing the wall temperature to 500K. The mechanisms of the loss generation can be found from the flow field shown in figure 2-7 through 2-9. The heat added from the casing wall is accumulated in the tip leakage vortices.

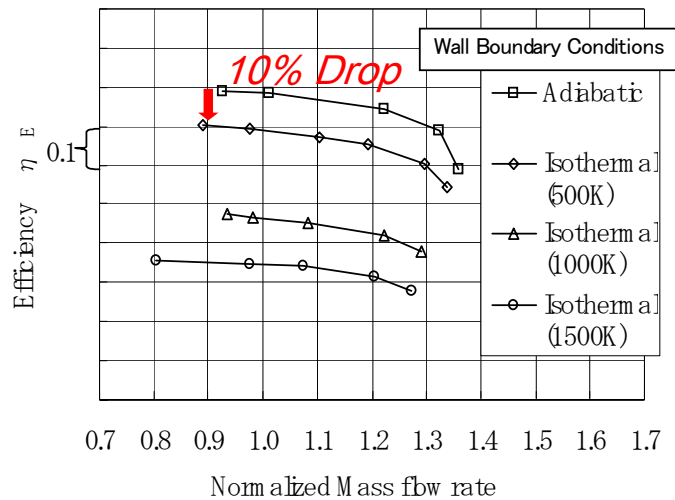


Figure 2-6: Effect of the Heat Addition on the Compressor Efficiency ($Re=1.41 \times 10^5$).

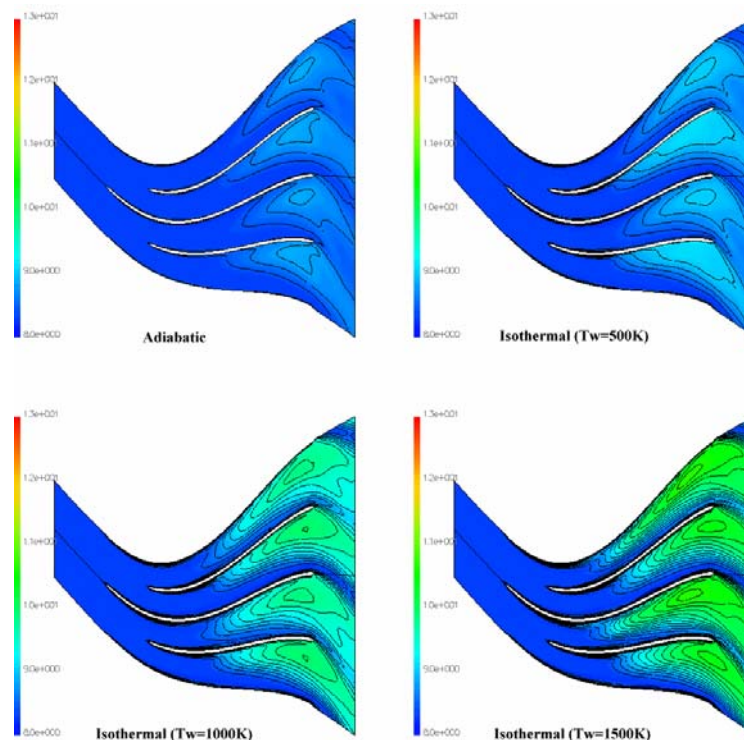


Figure 2-7: Entropy Contours in the 50% Blade-to-Blade Surface ($Re = 1.41 \times 10^5$).

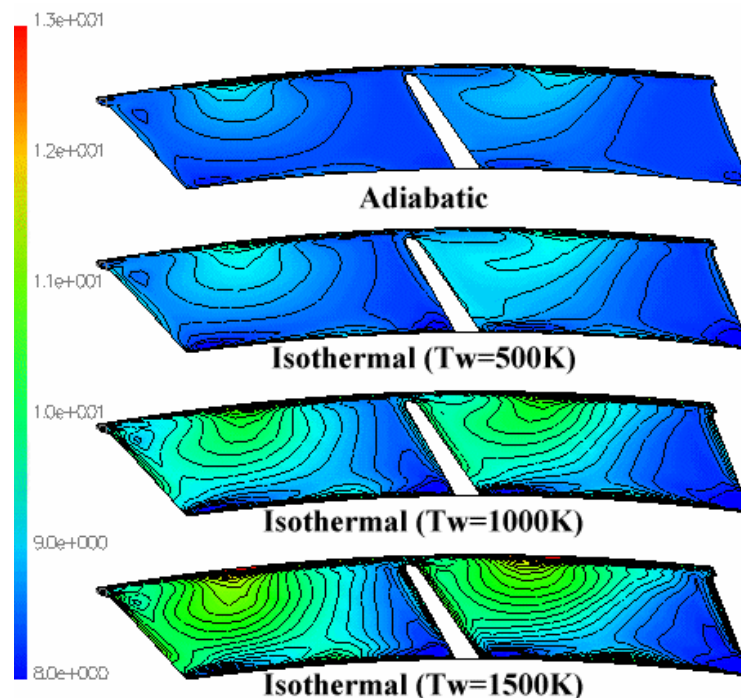


Figure 2-8: Entropy Contours in the Trailing Edge Surface ($Re = 1.41 \times 10^5$).

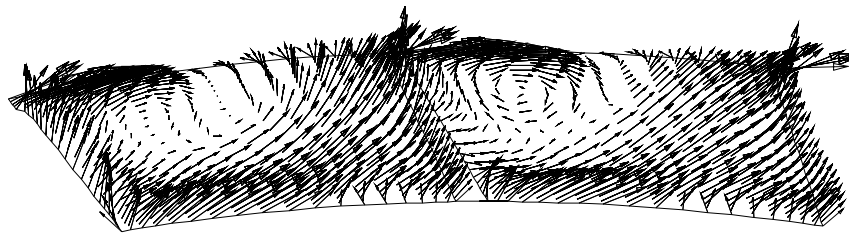


Figure 2-9: Velocity Vector at the Trailing Edge Plane
 $Re=1.41 \times 10^5$, 500K Isothermal Wall.

In micromachine gas turbines, the aerodynamics can be scaled, but the heat conduction cannot be. This is because the heat gradient depends on the material's property. Since the highest temperature, which is the combustor exit temperature, and the lowest temperature, which is the ambient temperature, in the micromachine gas turbine doesn't change much from those of large-scale gas turbines, it becomes harder to sustain the temperature difference by a wall, when the distance to separate those two temperatures reduces from an order of meters to an order of millimetres. Hence, the wall temperature of the compressor tends to increase when the dimension decreases, and this is one of the reasons why the efficiency of small gas turbines is lower in general, than that of larger gas turbines. At the ultimate small scale of the micromachine gas turbine, the heat isolation is one of the critical technologies to be developed.

The turbines have almost the same technical challenges as the compressors.

2.3 Bearings

In centrifugal compressors, pressure ratio is often expressed as a function of peripheral speed. To get higher pressure ratio, faster peripheral speed is required, and smaller diameter requires the impeller to

rotate faster. The trend of the impeller diameter and the rotating speed is shown in figure 2-4. The compressor of diameter 1cm is required to rotate at 870,000 rpm to generate pressure ratio 3.

To achieve this rotational speed, a bearing with very low friction loss is required. Its DN value (Diameter in mm multiplied by rotational speed in rpm) is 2,610,000 at the shaft diameter 3mm. This number is too large to realize with a miniature ball bearing. Therefore an air bearing is selected. One of the important technical issues in air bearing is its whorl stability. The plain bearing is inherently unstable unless a large side force is applied to keep the rotor offset to the journal. In a small machine with light-weight rotor, this implies a danger of easily losing the stability by disturbance. Therefore the bearing needs some mechanisms to enhance its whorl stability without side force. Some such mechanisms are herringbone groove, lobe shape or wave shape cross sections. These can be applied on either rotating axle or stationary journal. The differences of the stability due to different stabilizing mechanisms are shown in figure 2-10. Bearing Number is a non-dimensional rotating speed defined by $A=6\mu\omega(r/C)^2/Pa$. Dimensionless Mass Parameter is a non-dimensional maximum mass which the bearing can operate without whorl instability, and is defined by $M=mPaC^5/(2\mu^2br^5)$. The MEMS-GT is operable only in the region lower than the line for each type of bearing. The data from Dimofte [3] and Kobayashi [4] show the highest limit of the dimensionless mass parameter to allow stable operation of each type of the air bearing. The figure shows that stable operation at 870,000 rpm can be achieved by the herringbone bearing with grooved member rotating (GMR), or by the lobe type axle with the amplitude ratio $A_w=0.4$. The amplitude ratio (A_w) is the ratio of the lobe's peak-to-peak height divided by the average clearance between the axle and the journal. The herringbone type bearing provides relatively larger stable region compared to other types of hydrodynamic gas bearings. However, the required bearing clearance to operate in this region is smaller than 5 μm , and the appropriate selection of the fabrication method is required.

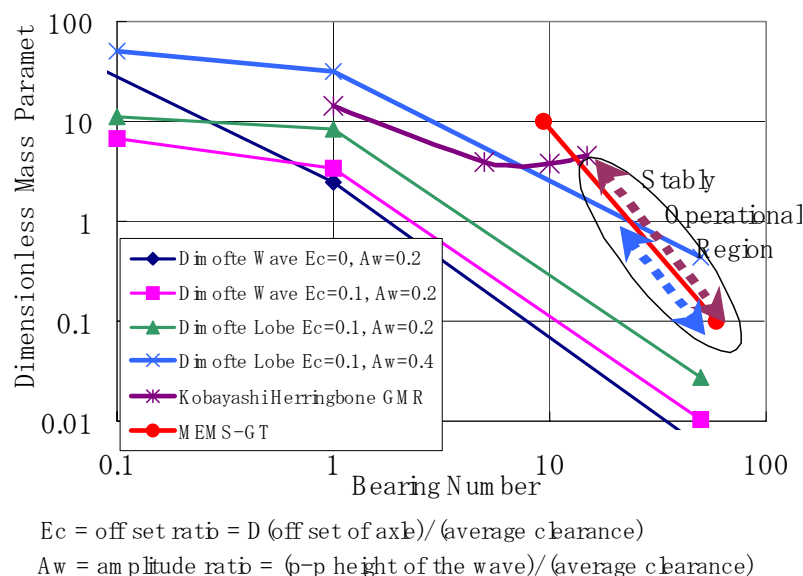


Figure 2-10: Stability of Various Hydrodynamic Gas Bearings.

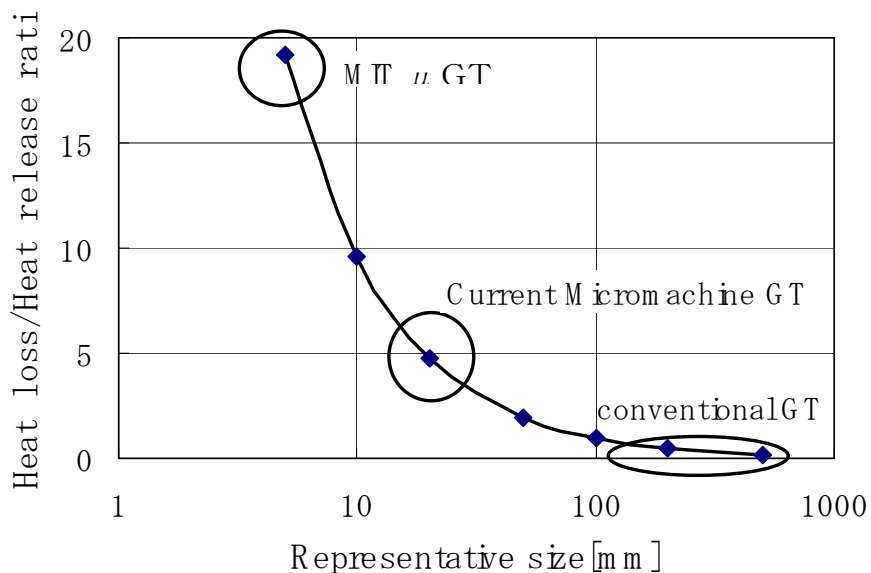
In addition to these mechanisms, the bearing should also be equipped with some static pressurizing mechanisms to add some side forces to enhance the stability, and to reduce the friction at the start up.

2.4 Combustor

The combustion phenomena of gases have their inherent length scale for the minimum height of the passage which the flame can be kept. This is called the quenching distance. To facilitate development of a

micro combustor, gas with the smallest quenching distance is chosen. That is Hydrogen. Its quenching distance is 0.6mm. Theoretically, Hydrogen combustor is feasible, if its length scale is larger than 0.6mm.

Even though it is feasible from a point of quenching distance, it will become difficult to sustain the flame when the length scale reduces, because the heat loss relative to the heat release increases. Here, the heat retention has been assessed. A simple sphere is used as a combustor model with its diameter being the representative size. The temperature of the inner wall and the outer wall are assumed to be $T_{w_{in}}=1000$ Celsius and $T_{w_{out}}=800$ Celsius, respectively. The wall thickness is fixed to 1mm regardless of the length scale, to remove the effect of the temperature gradient. The heat loss is modeled to be proportional to the surface area of the sphere, temperature gradient across the wall, and the heat conduction rate of the wall material. The heat release is modeled proportional to the volume of the sphere and the space heating rate. The space heating rate is a heat release divided by the combustor volume and the pressure. Therefore, the ratio of the heat loss to the heat release is proportional to inverse of the length scale, as is shown in figure 2-11. If the effect of larger temperature gradient due to thinner wall at smaller scale is added, the loss increase at smaller scale would be more. To keep the heat loss to heat release ratio not too large, the representative size of the combustor is selected to be about 15mm. At this scale of micromachine combustor, the heat loss to heat release ratio is expected to be about 5%. This is still an order larger than that of conventional gas turbines, but is much less than that of M.I.T., which is about 20% (Ref. [4]).



- Assumptions:- a sphere shaped combustor with single wall structure
 - inner temperature of combustor wall: 1000°C
 - inner/outer temp.[°C] ratio of combustor wall: $T_{w_{out}}/T_{w_{in}}: 0.8$

Figure 2-11: Heat Loss Rate of the Micro-Combustor.

Now the issue becomes whether the combustion can be sustained under these conditions of large heat losses. If the equivalence ratio increases over unity, the gas temperature starts falling, and at some point, the flame will be quenched. Therefore the equivalence ratio of unity is used as the criteria to assess the feasibility of the combustor. All the likely requirement of TIT gives the equivalence ratio under 0.5 as is shown in figure 2-12, over the range of the wall temperature ratio, which is the ratio of outer wall temperature to inner wall temperature. Therefore the micromachine combustor of representative size 15mm is shown to be feasible, and less risky to develop than M.I.T.'s micro combustor.

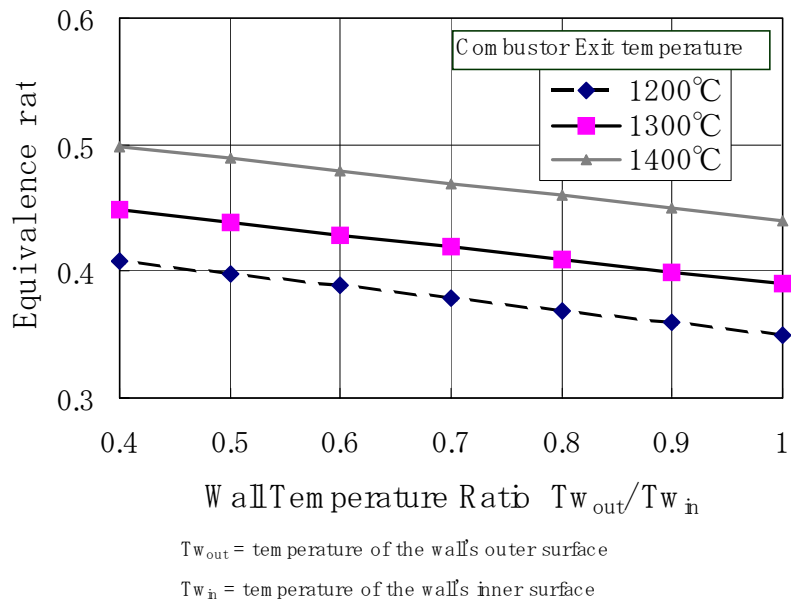


Figure 2-12: Equivalence Ratio to Keep the Wall Temperature.

2.5 Generator

The first issue on the generator is what type to choose, electromagnetic generator or electrostatic generator. Electromagnetic generator is a conventional type of generator that uses permanent magnets and electric magnets. Electrostatic generator is a type of generator that uses electric charges on the surface of the rotor and the stator. The image of the working principle and the example of a rotor is shown in Figure 2-13 and 2-14, respectively. From the figure, it is easy to understand that the electrostatic generator will work only at very small rotor to stator clearance, because electrostatic force due to the electric charge will decay inversely exponential to the distance and therefore it works only at very close distance. Hence, electrostatic generator suits only for a very small generator. Also, since electrostatic generator uses electric charges, it can generate large voltage at very close distance, but it won't be able to generate large current. In the other hand, the electromagnetic generator has limit in high-speed rotation. Those are the containment of the brittle magnets under large centrifugal force, and the increase of the iron loss at high frequency. The iron loss includes the eddy current loss and the hysteresis loss in the high-frequency switching of the current.

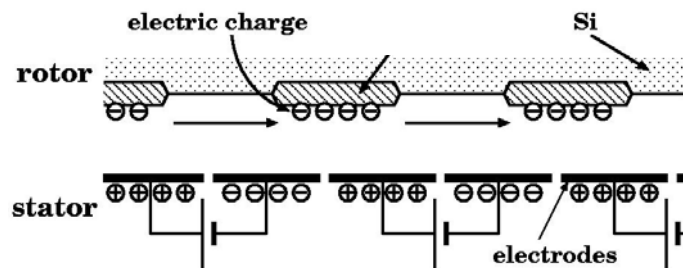


Figure 2-13: Working Principle of Electrostatic Generator.



Figure 2-14: An Image of the Rotor of Electrostatic Generator.

From 870,000 rpm of the rotating speed and the 10mm of the diameter, while considering the efficiency of voltage to current converter, electromagnetic generator has been selected as the baseline configuration. The technical challenge for developing the micro-generator is the containment, reduction of the loss, heat isolation to prevent the demagnetisation at the temperature beyond Curie point, and the rotordynamic integration with the turbine.

3.0 COMPONENT DEVELOPMENT

3.1 Compressor & Turbine

A micro-turbocharger has been designed and fabricated. Its cross sectional drawing and the fabricated rotor are shown in Figure 3-1 and 3-2, respectively. The micro-turbocharger is used as a combined test rig for the compressor and the bearing to prove their performance without the effect of heat transfer. The specification of the turbocharger is shown in Table 3-1. Here, the turbine is just a driver, and therefore is larger than the compressor to ensure enough power to drive the compressor and the bearing at high speed. The inflow to the turbine is mildly heated by an electric heater to increase the enthalpy of the driving gas. The rotor is made of titanium (*Ti-6Al-4V*). The rotor assembly is designed to run above the first and second rigid mode vibration, but below the first bending mode vibration, at the design speed.

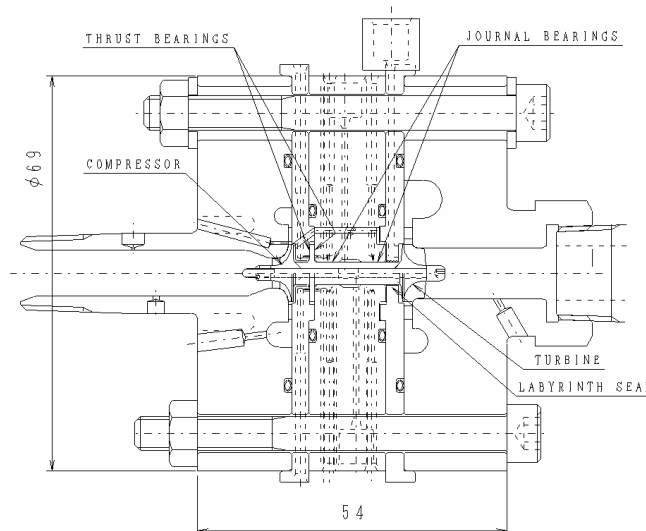


Figure 3-1: Designed Micro-Turbocharger.

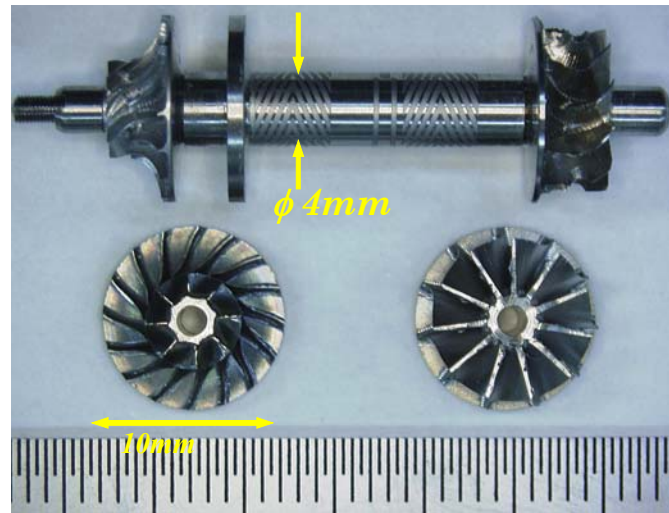


Figure 3-2: Fabricated Rotor of the Micro-Turbocharger.

Table 3-1: Major Specifications of the Micro-Turbo Charger

	Compressor	Turbine
No. of Blades	8+8	11
No. of Vanes	15	12
Diameter	10mm	
Rotational Speed	870,000rpm	
Pressure Ratio	3.0	4.0
Inflow Temp.	288K (15 Celsius)	393K (120 Celsius)
Outflow Temp	444K (171 Celsius)	367K (94 Celsius)
Mass Flow Rate	2g/s	13.4g/s

Two types of the rotor have been developed; i.e. the rotor for hydroinertia gas bearing, and the rotor for hydrodynamic gas bearings. The rotor for hydrodynamic gas bearings has herringbone grooves on the shaft for the journal bearings, and has spiral grooves for the thrust bearings. The herringbone grooves and the spiral grooves are formed by MEMS fabrication method. Especially, the herringbone grooves are etched on the cylindrical surface of the shaft of diameter 4mm. A method to etch on a cylindrical surface by slowly rotating the shaft on a flat plate mask while projecting a thin sheet of light has been developed. In addition to these dynamic gas bearings, static gas bearings are added to jack-up the rotor during the starting-up and stopping operations. The surface of the shaft is covered with chrome nitride (CrN) coating to prevent the burning of the metal surface in the case of surface contact. The stationary parts of the turbocharger are made of SUS403 that has about the same thermal expansion rate as titanium.

The rotor has a conventional tie-bolt construction to connect the impellers to the shaft. The conical faces at the both end of the shaft fix the position of the impellers. All the parts to for the rotor are shown in Figure 3-3. The validity of this construction, especially under the effect of the deformation of the conical face due to the centrifugal force has been assessed by FEM calculations. The results are shown in Figure 3-4 and 3-5. Figure 3-4 shows the shape of the deformation occurred in current rotor, due to the centrifugal force

at the design rotational speed, 870,000 rpm, with different axial displacement by the tie-bolt. The relation of the axial displacement and the axial load is shown in Figure 3-5. This axial load is generated by the tie-bolt, and the construction works only if the axial displacement of the tie bolt is larger than that of the shaft. If the axial displacement of the tie-bolt is smaller than that of the shaft at a certain axial load, this means that the tie bolt won't work. The figure shows that the tie-bolt construction works by applying the tensile force larger than 150N to the tie bolt.

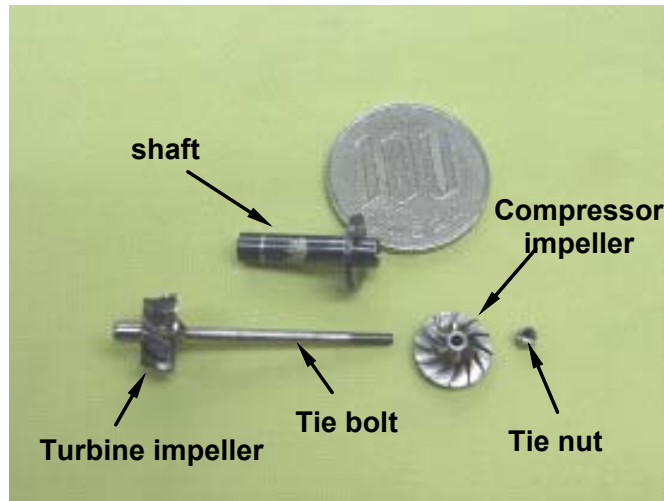


Figure 3-3: All the Parts of the Micro-Rotor (with a shaft for hydroinertia gas bearings).

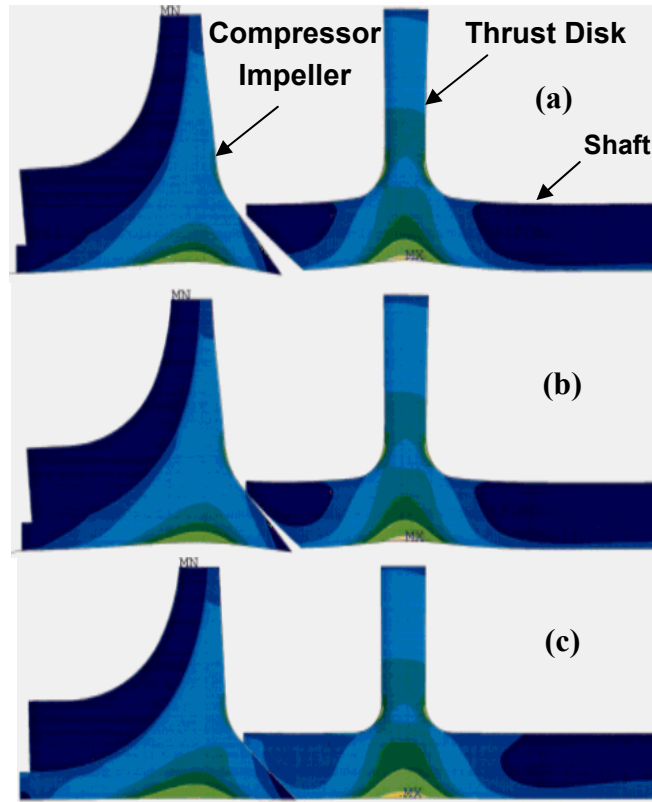


Figure 3-4: Strain Distribution and Deformation of the Shaft at 870,000 rpm.

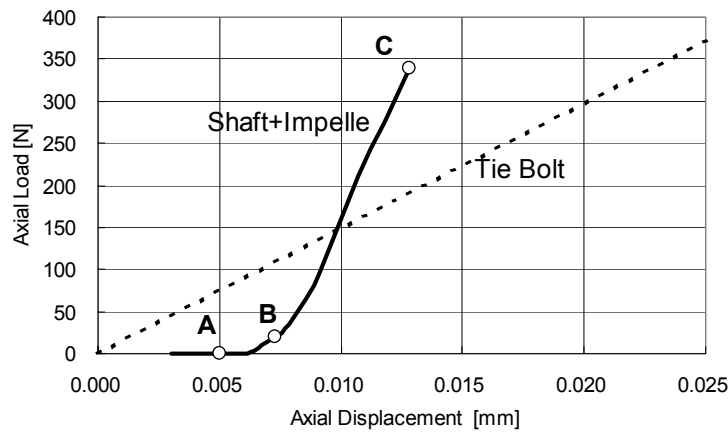


Figure 3-5: Elongation of the Tie Bolt.

The details of the measurement system in the turbocharger are tabulated in Table 3-2. Nine temperatures, eleven pressures, four volume flow rates, two shaft vibrations, and a rotation speed are measured. The rotational speed and the shaft vibrations are measured by laser optical probe of diameter 0.8mm. The turbocharger set up with the measurement system is shown in Figure 3-6, and the close-up view of the micro-turbo charger without turbine casing is shown in Figure 3-7.

Table 3-2: Measurement Points in the Micro-Turbo Charger

Static Pressure	Compressor in/out Flow meter in/out between compressor rotor and stator exit scroll Turbine in/out Flow meter in/out Bearing bypass	Miniature pressure transducer
Temperature	Compressor in/out Flow meter in/out exit scroll Turbine in/out Flow meter in/out Journal Bearing x 2	φ1mm K-type Thermo couple
Volume Flow Rate	Compressor in/out Turbine in/out	Flow meter
Vibration	Displacement radial (shaft) Axial (Turbine back face)	φ0.8mm Laser probe
Rotational Speed	1/rev groove on shaft	

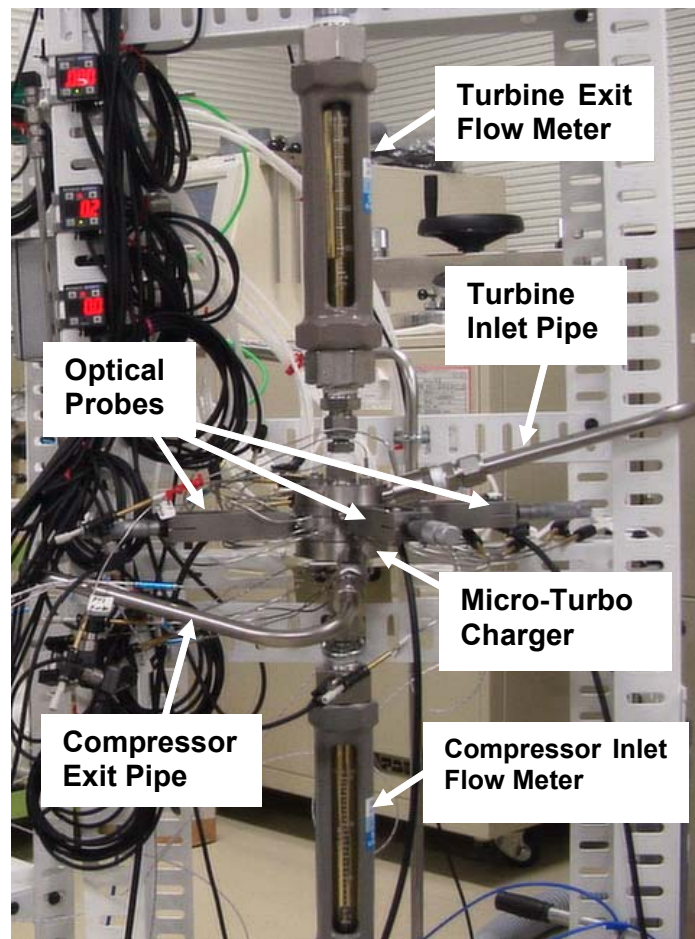


Figure 3-6: Test Set Up of Micro-Turbo Charger.

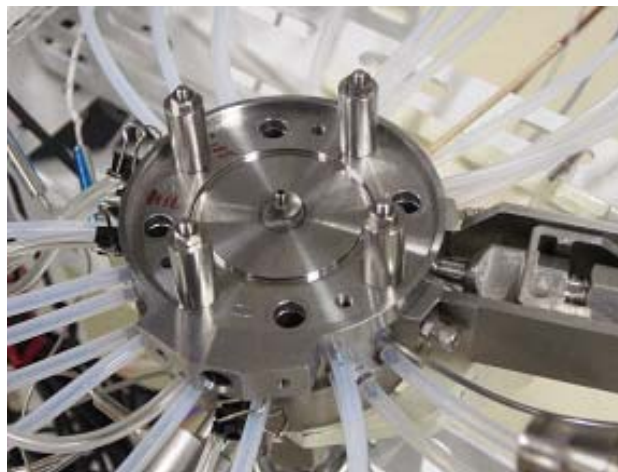


Figure 3-7: Close-up View of the Micro-Turbo Charger without Turbine Casing.

Figure 3-8 (a) and (b) show the adiabatic efficiency and the pressure ratio of the compressor (compressor diagrams), respectively, measured by a micro-turbo charger test using hydroinertia bearings. The compressor maps were obtained at about 50 % (435,000 rpm) and 60 % (520,000 rpm) of the design speed. The measured pressure ratio is lower than estimated value. This could be due to both the heat dissipation

from the wall, and the impeller tip clearance being larger than the designed value of 25 μm . In this study, the impeller tip clearance was set large enough to prevent the impeller tip from crashing to the shroud. The machining error of the impeller and shroud were not within the required tolerances, and also the large bearing clearance of the hydroinertia gas bearings allows large radial displacement of the impellers located at the both end of the shaft.

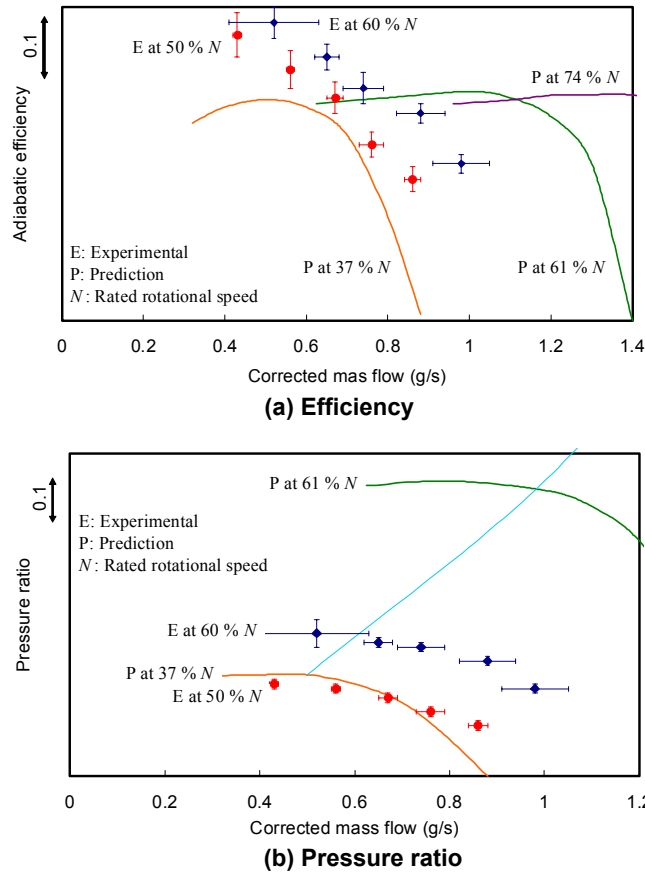


Figure 3-8: Measured Compressor Performance Map.

The measured adiabatic efficiency shows unrealistically high values. This is mainly due to the heat dissipation from compressed air. Compressor adiabatic efficiency, η_c , is the ratio of required adiabatic work calculated from measured pressure ratio to actual work calculated from measured temperature ratio, and is given by

$$\eta_c = \frac{\pi_c^{(\gamma-1)/\gamma} - 1}{T_{C_{out}} / T_{C_{in}} - 1}, \tag{3.1.1}$$

where π_c is pressure ratio, $T_{C_{in}}$ and $T_{C_{out}}$ are inlet and outlet temperature, respectively, and γ is specific heat ratio. $T_{C_{out}}$ tends to be measured lower than the resulting temperature due to the actual work given by the rotor. The sources of this error are the heat dissipation from the shroud, the duct walls, and the sheath of the thermo couple. The first two effects will lower the real temperature of the flow, and the third effect causes the measurement error. Hence, the actual compressing work is underestimated, so that adiabatic efficiency is overestimated from the above equation. In the other hand, the adiabatic efficiency of turbine tends to be underestimated by the same reasons. The turbine efficiency is given by

$$\eta_T = \frac{1 - T_{T_{out}} / T_{T_{in}}}{1 - \pi_T^{(1-\gamma)/\gamma}}, \quad (3.1.2)$$

where subscript ()_T indicates the values for turbine. Note that π_T is defined as

$$\pi_T \equiv \frac{P_{T_{in}}}{P_{T_{out}}}. \quad (3.1.3)$$

Actions to be taken to improve the accuracy of the efficiency measurement of micro compressor will be as follows:

- (1) Improve the heat shielding by using material with lower heat conductivity;
- (2) Reduce the heat dissipation by reducing the capacity of the heat flow path;
- (3) Use the thinner thermocouple to reduce the heat flow through the sheath;
- (4) Install the thermocouple heading upstream to reduce the temperature gradient in the sheath around the thermocouple;
- (5) Wait long enough (may be more than an hour!) before each measurement to confirm the thermal equilibrium; and
- (6) Evaluate the efficiency by the product of the compressor efficiency and the turbine efficiency to offset the heat dissipation effect.

3.2 Bearings

A micro-bearing tester has been designed and fabricated to develop the bearings to realize stable operation at 870,000 rpm. The bird eye views and the cross sectional view of the tester are shown in Figure 3-9 and 3-10, respectively. The micro-rotor is shown in Figure 3-11. The rotor of diameter 4mm has a thrust disk of diameter 10mm at the center of the shaft, with two journal bearings at the symmetric position to the thrust disk. The rotor is driven by a centrifugal turbine of diameter 10mm, which is located at an end of the shaft, and a dummy compressor is located at the other end of the shaft. The dummy compressor is a cylindrical shaft that is designed to have the same mass and moment of inertia to the compressor for the expected micro-machine gas turbine hence the rotor has the same rotor dynamic characteristic to the rotor for the gas turbine.

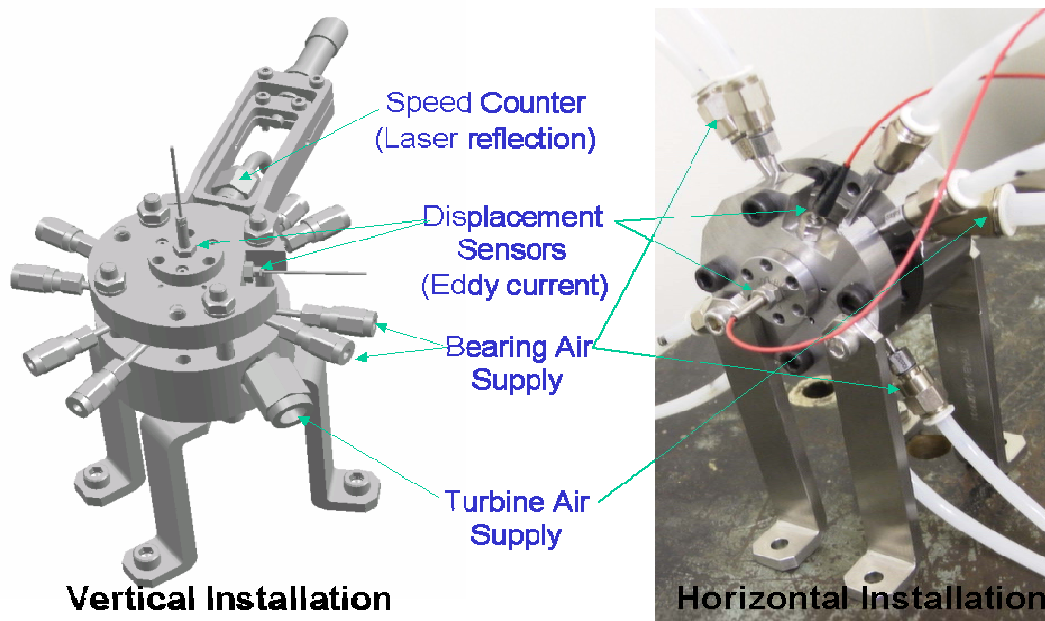


Figure 3-9: Bird-Eye View of the Micro-Bearing Tester.

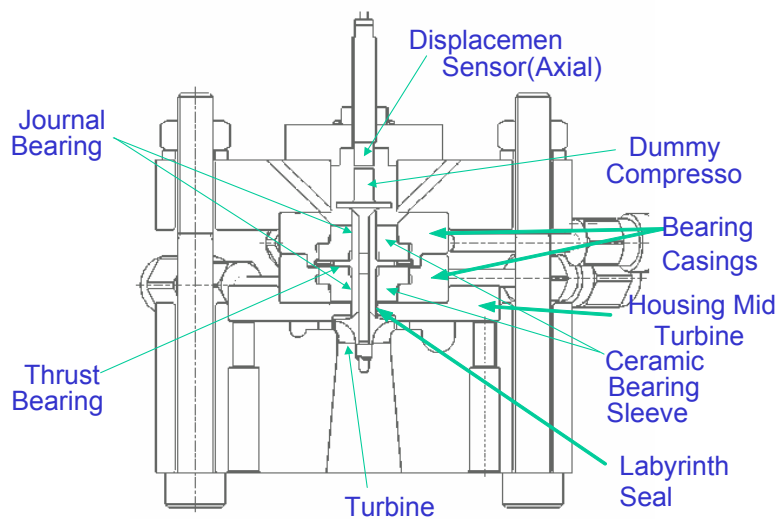


Figure 3-10: Cross Sectional View of the Micro-Bearing Tester.

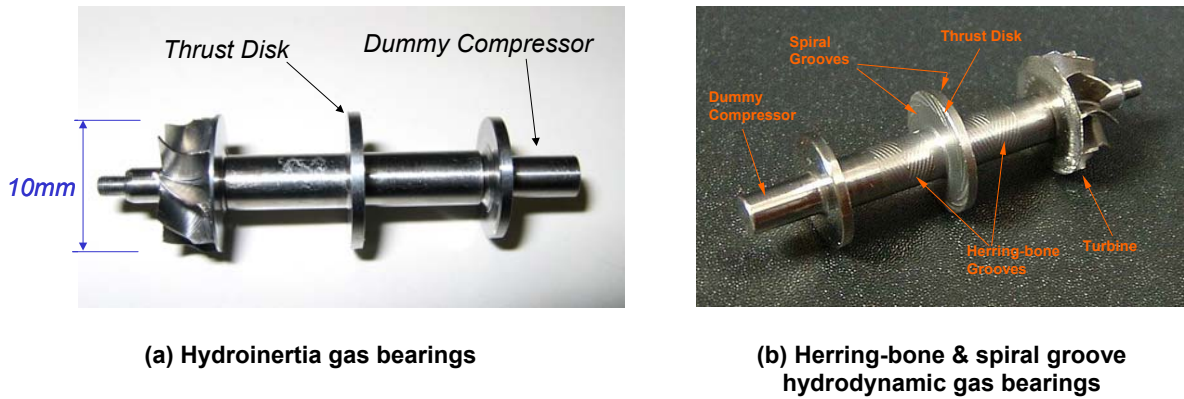


Figure 3-11: Micro-Rotor.

The rotor has a conventional structure of high-speed turbo machines that the shaft and the impeller are connected by a tie-bolt. The diameter of the tie-bolt is 1.6mm. The rotor is made of titanium (Ti-6Al-4V), and weighs 2.3g. The shaft is coated by CrN ceramic of 3µm thick to increase the durability in the case that the rotor touches the bearing sleeve during the operation.

The bearing sleeves are made of Zirconium (ZrO₂) ceramic. The selection of Zirconium ceramic is also to increase the durability of the bearing sleeves in the event of the rotor touching the bearing sleeves. The bearing will easily be burnt even by a slight contact of the rotor and the bearing sleeves, if both sides are not made of ceramics. Each bearing has 8 holes of diameter 0.3mm to feed the bearing gas. The supply pressure can be changed independently for each bearing.

The hydroinertia gas bearings and hydrodynamic gas bearings with Herring-bone & Spiral grooves are tested with this bearing tester. The vibrations of the shaft are measured at dummy compressor, one in radial direction, and the other in axial direction, by eddy current displacement sensor of diameter 3mm.

The maximum speed of 770,000 rpm has been successfully achieved by hydroinertia gas bearings. The vibration data are shown in Figure 3-12. The whirl ratio has been measured to be 9. The bearing test will be continued until the method to achieve stable operation at the design speed of 870,000 rpm is established.

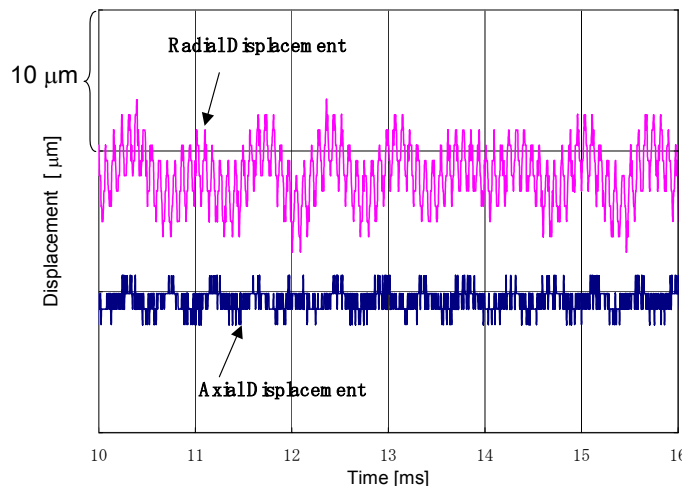


Figure 3-12: Shaft Vibration at 770,000 rpm.

3.3 Combustor

Two types of microcombustors have been considered. One type is a canister type combustor, which is a scale down of typical combustors for modern gas turbines. The flow paths between the combustor and the compressor, and turbine are connected by scroll. The merit of this type of combustor is that the surface to volume ratio can be minimized, therefore the heat can be retained relatively easy, and the length scale of the burning region can be maximized for the volume. Thus high combustion efficiency can be expected. Also, this configuration has geometrical advantage on heat isolation between compressor and the combustor. In the other hand, the existence of the scrolls will make the flow passage long, and make the system complicated and large. The other type is a doughnut type combustor similar to the type under development at Massachusetts Institute of Technology (MIT)[5]. This type of combustor has a merit in its compactness, and suitability for manufacturing by MEMS batch process, in future.

Both type of combustors are designed and built at semi-microscale at twice the mass flow rate of the target scale. This is to ease the realization of the self-sustained flame to measure the discrepancy of the character of the flame from the predicted values, due to the scale effect. The specifications of the both type of semi-microcombustor are shown in figure 3-13(a) and (b). The canister type combustor consists of combustor vessel, air swirler, fuel nozzle, igniter, and combustor liner with twelve dilution holes. The combustor liner is cooled by external convection and film cooling flow. The igniter consists of anode wire and ceramic tube. The spark ignition energy is supplied by piezo-electric element of gas lighter on market. The doughnut-type combustor doesn't have the liner. Because of the lack of the liner and the large surface to volume ratio, the doughnut type combustor is expected to have higher heat dissipation than canister-type combustor.

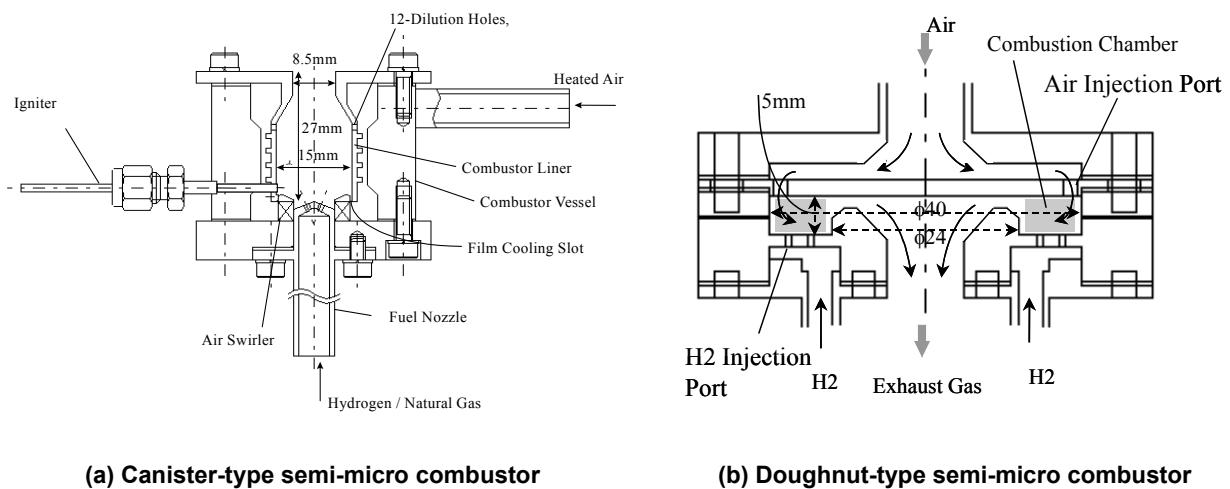


Figure 3-13: Double-Scale Semi-Micro Combustors (x2 scale).

The experiments with hydrogen fuel have been performed for both canister-type and doughnut-type combustors. Stable ignition and self-sustained stable combustion were achieved under all the test conditions. The test conditions spanned from 0.2g/sec to 2.2g/sec of air flow rate, and from 0.003g/sec to 0.03g/sec of hydrogen fuel flow rate, which correspond to the range of the flow meters.

The exhaust gas temperature distributions of the both combustors are measured by R-type thermo-couple located 1mm downstream of the combustor exit. The results in figure 3-14 show approximately 300K lower temperature for the doughnut-type combustor. The canister-type combustor shows the exit temperature close to the design value (1050 Celsius), but the doughnut-type combustor shows significantly lower exit temperature. The heat loss is estimated to be approximately 20% for the doughnut-type combustor, and approximately 1.2% for the canister-type combustor. The doughnut-type combustor may

have geometric benefit in two-dimensional gas turbine made by MEMS fabrication process, but it has shown rather poor thermodynamic performance. In the other hand, the canister-type combustor has not shown any significant problems. Therefore, the canister-type combustor has been selected as the baseline combustor for the gas turbine made by 5-axis micro-end mill.

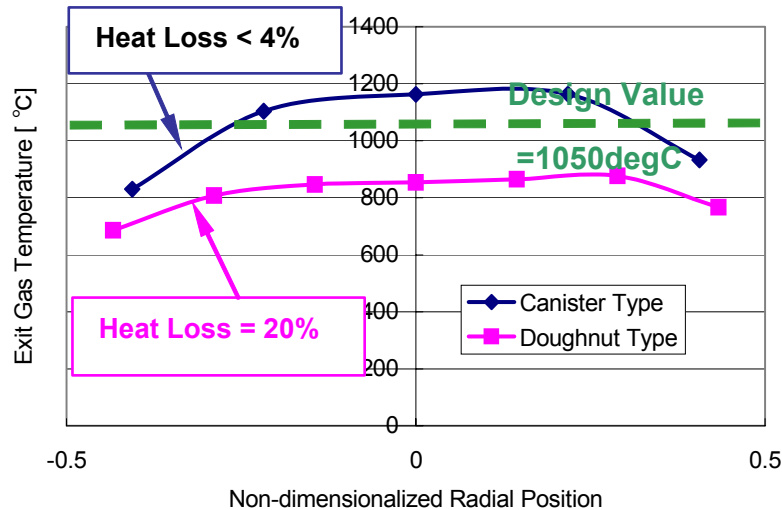


Figure 3-14: Exhaust Gas Temperature Distribution of Semi-Micro Combustor.

Based on the results of the double-scale models, canister type micro-combustors for both hydrogen fuel and methane fuel have been designed and tested. The specifications of the both micro-combustors are tabulated in Table 3-3.

Table 3-3: Design Conditions of the Micro-Combustors

Fuel	Methane	Hydrogen
Air flow rate	2.0 g/s	
Inlet pressure	304 kPa	
Inlet temperature	444 K	
Exit temperature	1323 K	
Equivalence ratio	0.37	0.28
Liner Volume	16.9 cm ³	2.01 cm ³
Duration time	6.5 msec	0.72 msec

The hydrogen micro-combustor has approximately 2 cc of capacity, and it has successfully achieved 99.9 % of the combustion efficiency (Figure 3-15) after experiments with several different fuel nozzles. The micro-combustor for methane fuel has approximately 17 cc of capacity, and it has also achieved 99.9 % of combustion efficiency experimentally (Figure 3-16). The methane micro-combustor achieved approximately 20 ppm of NO_x emission, which suggests that the methane micro-combustor can be used without extra treatment to reduce the emission.

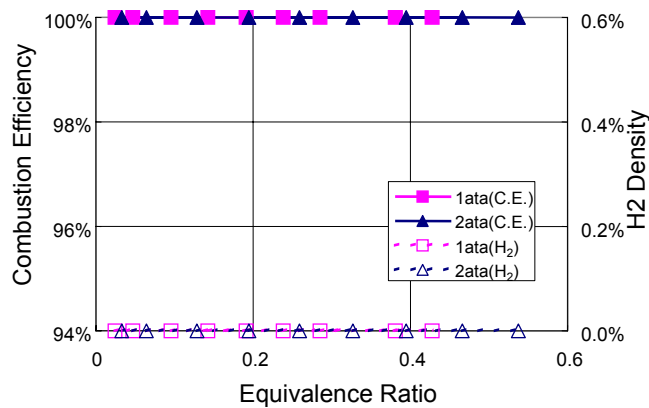


Figure 3-15: Combustion Efficiency of the Micro-Combustor with Hydrogen Fuel.

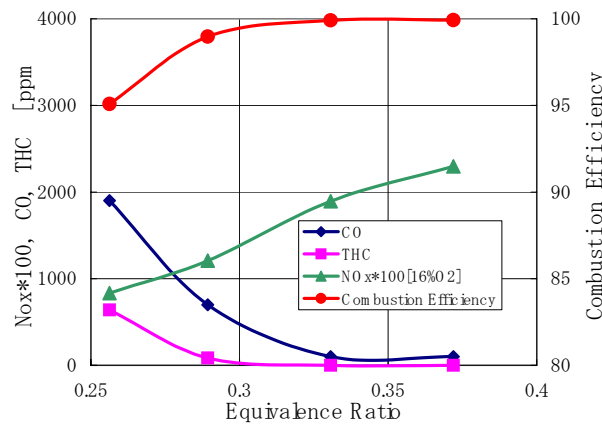


Figure 3-16: Combustion Efficiency of the Micro-Combustor for Methane Fuel.

Both combustors have significantly different size. The combustors were designed by approximately matching the loading parameter to large-scale combustors. The reaction time of hydrogen is assumed to be approximately 10 times faster than that of methane. The test results showed wider range of equivalence ratio to provide the combustion efficiency higher than 99.9 %. This suggests that the size of the hydrogen micro-combustor can further be reduced from current size, 2 cc.

3.4 Generator

The technical challenges in developing the micro-generator are the development of the structure to contain the brittle magnet, and the method to reduce the iron loss at high-speed operation. To achieve the goal, bi-polar rotor with 3-phase 6-slot stators configuration has been selected to reduce the electric frequency, with Samarium-Cobalt magnet that has strong magnet force even at relatively high temperature, for the permanent magnet. The magnet is tight-fit in the rotor shaft to obtain the containment capability without increasing the diameter. The construction of the designed micro-generator based on these requirements is shown in Figure 3-17. Two ball bearings are used for the initial development. Hence the maximum rotating speed is limited to 400,000 rpm. Even with bi-polar rotor, the electric frequency at the design speed of 870,000 rpm will become as high as 14.5KHz. Hence, the selection of the core material to minimize the iron loss becomes important, and a test machine has been fabricated to test variety of core material to down select the best material. The fabricated test machine is shown in Figure 3-18. Three different cores are tested. Those are; (a) 0.1mm thick Si-steel sheet, (b) 0.05mm thick Si-steel sheet,

and (3) Ferrite. Ferrite is selected because of its low iron loss. Si-steel is selected due to its capability for high precision machining that more sophisticated core shape can be realized.

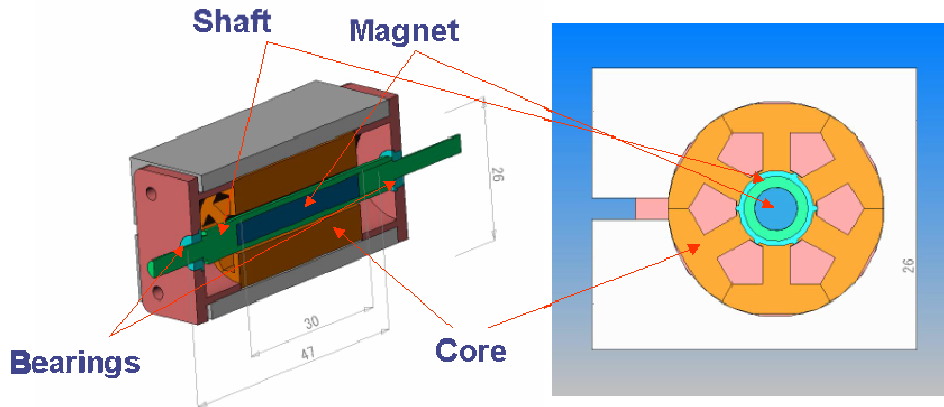


Figure 3-17: Structure of the Micro-Generator.

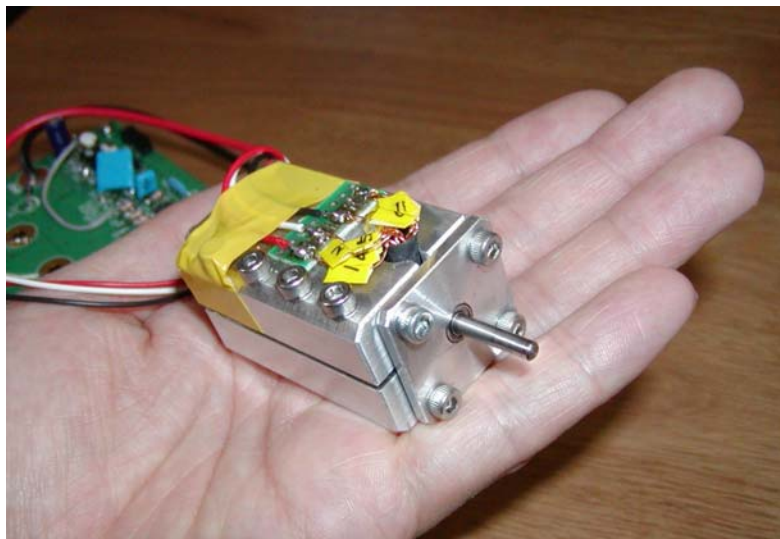


Figure 3-18: Fabricated Micro-Generator Test Model.

The test to check the quality of the back electromotive force has been conducted. The resulting voltage outputs are shown in Figure 3-19. The Si-steel core showed clean sinusoidal waveform while that of ferrite core showed some wiggle. This is due to the difference in the core shape. Si-steel cores have bumps to reduce the spaces between the adjacent cores to reduce the variation of the magnetic flux density in the gap between the rotor and the stator, while ferrite core doesn't have them.

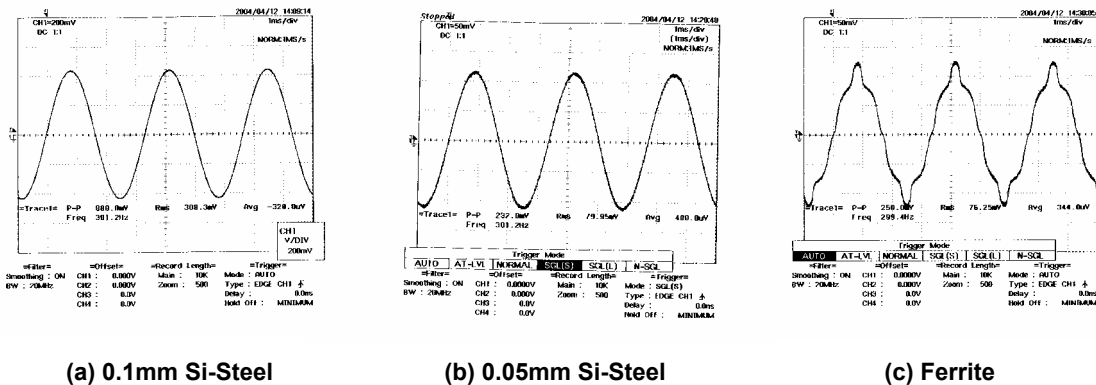


Figure 3-19: Output Voltage Waveform with Different Stator Core Materials.

Next, the rotating loss is measured by driving the micro generator by another motor and measuring the power required to drive the motor. The test is performed only at low speeds because of the limit of drive motor’s capability. The iron loss characteristics and the test results are tabulated in Table 3-4, as relative values to the 0.1mm Si-steel sheet core data. It is seen that the 0.05mm Si-steel sheet core showed the smallest loss, and the ferrite core showed the largest loss, although the iron loss characteristics of the ferrite core is the smallest. Although the differences are very small, and since the tested speeds are less than 3% of the design speed, no conclusions can be derived from these results, yet.

Table 3-4: Iron Loss and Tested Rotating Loss of the Core

Core configuration		(a) 0.1mm Si-steel sheet	(b) 0.05mm Si-steel sheet	(c) Ferrite
Iron loss of the material		300W/kg	200W/kg	41W/kg
Rotating loss (tested)	12,000rpm	100	105.8	105.8
	18,000rpm	100	103.3	103.3
	24,000rpm	100	97.9	104.2

Finally, the generator is driven as an electric motor to verify the performance of the electric circuit. The rotor has successfully been driven up to 170,000 rpm, until the voltage limit of the electric circuit has prevented the test from going higher. The rotordynamic character has been verified to be able to drive up to this speed. The development will be continued to test the generator at higher shaft speed by modifying the driving methods, from electric motor to air turbine, for example.

4.0 FABRICATION TECHNOLOGY DEVELOPMENT

Although we chose to develop a three-dimensional gas turbines based on the modern technologies for the large scale gas turbines, the gas turbines at micro-scale may not be able to be fabricated only by existing fabrication technologies. Hence, in the project, variety of fabrication techniques have also been developed.

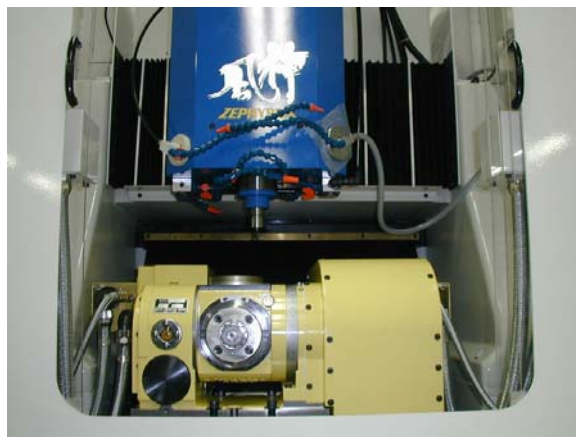
4.1 Micro-Milling of the Impeller

The compressor and the turbine impellers are machined by a five-axis NC milling machine (Toshiba Machine Co., Ltd, F-MACH with an additional rotating stage) shown in Figure 4-1, using a tapered ball

end mill with a diameter of 0.5 mm and a taper angle of 3 degrees (NS Tool Co., Ltd, MTB230). For finishing a compressor impeller made of titanium, about 60 hours are needed in machine time, because cutting depth and feed rate are set small enough to prevent the thin tool from breaking. As a result, the surface of the impeller is well finished using only three tools from rough cutting. The machined impellers are shown in Figure 4-2.



(a) Outlook of the system



(b) Close-up view of the working stage

Figure 4-1: Five Axis NC Milling Machine.

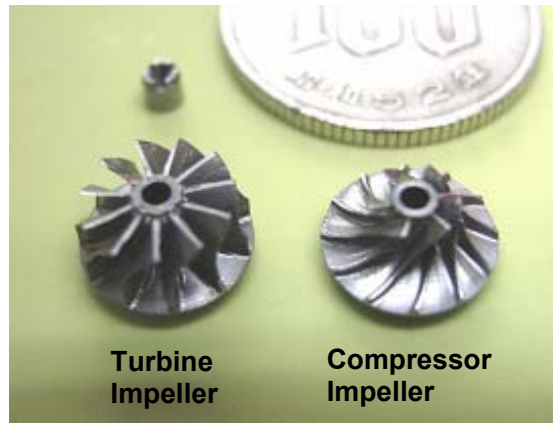
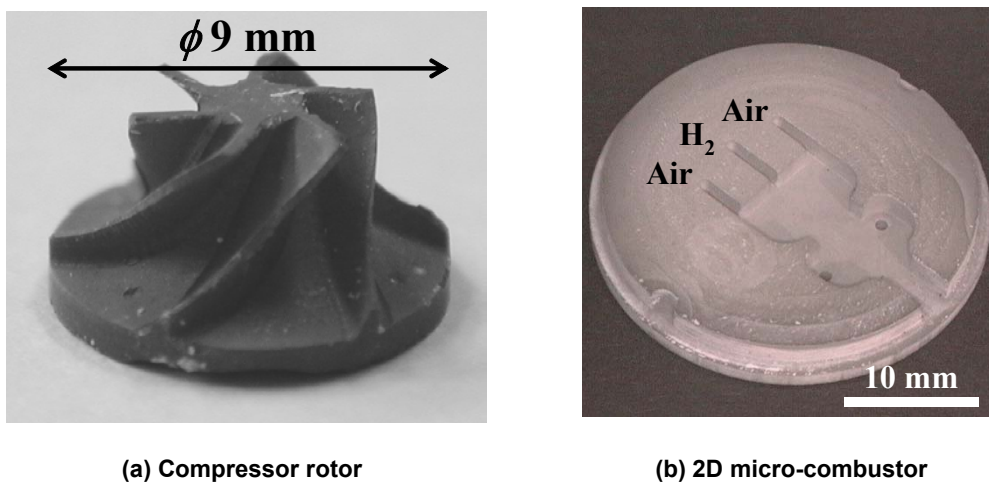


Figure 4-2: Fabricated Compressor and Turbine Impellers.

4.2 Fabrication of the Impeller by Micro Machining of Silicon Nitride (Si_3N_4)

Silicon nitride (Si_3N_4) is a heat-resistive material, which especially has excellent thermal shock resistance. We have developed the mechanical micromachining technology of Si_3N_4 ceramic [6]. The process can be briefly described as a silicon green compact formed by spark plasma sintering (SPS) is reaction-sintered in nitrogen atmosphere after being mechanically micromachined. In the first step, a silicon green compact is prepared from silicon powder by SPS. SPS uses pulse direct current during sintering to form a dense sintered body at relatively low temperature in short time with good repeatability. SPS is suitable to form the silicon green compact, because the density of final Si_3N_4 ceramic depends on the density of the silicon green compact. A Si_3N_4 density of about 90 % is obtained by SPS at 1300 °C and 20 MPa. Next, the silicon green compact is mechanically micromachined using a high speed milling machine shown in Figure 4-1. Finally, the shaped silicon green compact is nitrided in 10 MPa nitrogen atmosphere at 1330 °C to be converted into Si_3N_4 ceramic. The shrinkage ratio of the Si_3N_4 ceramic from the silicon green compact is as small as 1 ~ 3 %, and near-net-shaping is possible.

Figure 4-3 shows Si_3N_4 ceramic parts fabricated by this process. The turbine impeller with a diameter of 9 mm (Fig. 4-3 (a)) demonstrated the potential of this process to fabricate complicated 3-dimensional structures. The 2-dimensional microcombustor (Fig. 4-3 (b)) was tested using hydrogen fuel, and realized power density as high as 2 GW/m³ [7]. The combustion temperature rose to 1000 ~ 1500 °C, but no damage was observed in the microcombustor.



(a) Compressor rotor

(b) 2D micro-combustor

Figure 4-3: Fabricated Parts by Machining of Silicon Nitride.

4.3 Fabrication of the Impeller by Micro Reaction Sintering of Silicon Carbide (SiC)

To manufacture heat-resistive microparts for the miniature gas turbine generator etc., we have developed a novel method to reaction-sinter 3-dimensional SiC microstructures using micromachined silicon molds [8]. Figure 4-4 shows the process: 1) micromachining silicon molds, 2) filling the molds with material powders composed of SiC, graphite and phenol resin, 3) reaction-sintering by hot isostatic pressing (HIP) at 1500 ~ 1700 °C, and 4) releasing a SiC product from the silicon molds by wet etching. Figure 4-5 shows a silicon mold and a SiC rotor with a diameter of 5 mm fabricated using the silicon mold. The shape of the silicon mold was well transferred to the SiC product within 3 % shrinkage. X-ray diffraction (XRD) analysis revealed that SiC was newly produced by the reaction between silicon and graphite in the reaction-sintering. SiC from this process has approximately 70% bending strength and 70 ~ 80 % Vickers hardness compared to those of a commercially-available reaction-sintered SiC.

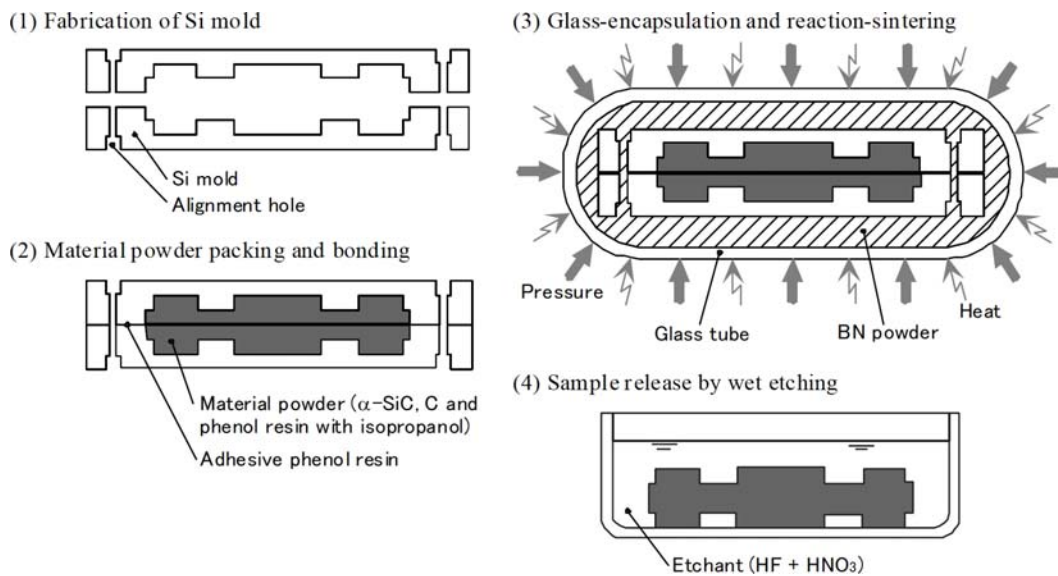


Figure 4-4: The Process of SiC Micro Reaction Sintering.

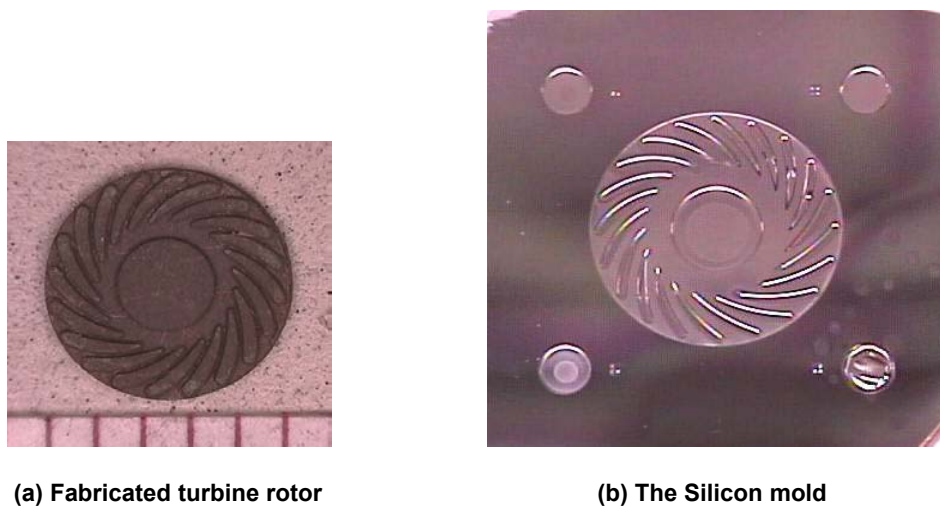


Figure 4-5: 2D Turbine Impeller made by SiC Micro Reaction Sintering.

4.4 Etching of the Herring-Bone Grooves and the Spiral Grooves on a Shaft

Figure 4-6 shows the shaft with bearing grooves fabricated by photolithography and wet etching. The herring-bone grooves on the cylindrical surface are fabricated using a special maskless exposure system with a rotating sample stage (Ball Semiconductor). Positive photoresist (Clariant, AZ 4400) is uniformly spread on the cylindrical surface by dipping the shaft into the photoresist and suspending it in solvent vapor. The image of the herring-bones is generated on a Digital Micromirror Device (Texas Instruments) in the maskless exposure system, and projected to the cylindrical surface by rotating the shaft step by step. After development and hard baking, the shaft is wet-etched by the mixture of fluoric acid and hydrogen peroxide.



(a) General view of the etched rotor



(b) Close-up view of the Herring-bone and Spiral grooves

Figure 4-6: Herringbone & Spiral Grooves Fabricated on the Shaft.

To fabricate the spiral groove on the thrust disc, the photoresist is first spread on the shaft by spinning the shaft. The spiral groove pattern is transferred using a special photomask with a hole where the shaft passes, and then the shaft is wet-etched by the same method to that for Herring-bone grooves. By repeating these steps, the spiral grooves are fabricated on both sides of the thrust disc.

5.0 SUMMARY

5.1 What We Achieved

- 1) The cycle to realize the 100W micromachine gas turbine generator and the requirements for each component has been specified.
- 2) The feasibility of the micro-combustor has successfully been validated by experiment, for hydrogen fuel and methane fuel.
- 3) The micro-compressor has been developed, and performed the aerodynamic performance measurements, up to the 55% of the design speed.
- 4) The micro-bearing test rig has been developed, and successfully ran up to 770,000 rpm, which is the record high speed for the configuration for micromachine gas turbines.
- 5) The micro-generator has been designed, and tested up to 170,000 rpm.

5.2 Remaining Issues and Future Schedule

- 1) The effort to achieve the design speed of 870,000 rpm will be continued to establish the method to increase the whirl ratio.
- 2) The development of the generator will be continued to clarify the high-speed limit for the practical use.
- 3) Based on the limitations of component technologies found from the component tests, and the requirement of the market, the specification of the micromachine gas turbine generator will be reviewed to move into the development of the production machines.
- 4) The development of the micro-recuperator is desired, to improve the thermal efficiency of the micromachine gas turbines.

REFERENCES

- [1] “Trend Report on Development of High Density Miniature Power Source Technologies”, New Energy and Industrial Technology Development Organization, March 2001 (in Japanese).
- [2] Isomura, K., et al, “Feasibility Study of a Micromachine Gas Turbine”, ASME 2001-GT-101, June 2001.
- [3] Demofte, F., “Wave Journal Bearing with Compressible Lubricant – Part2: A Comparison of the Wave Bearing with a Wave-Groove Bearing and a Lobe Bearing”, STLE Tribology Transaction Vol. 38, No. 2, pp. 364-372, 1995.
- [4] Kobayashi, T., “Dynamic Analysis of Wave Shape Gas Journal Bearings – Comparison with Bearings with Herringbone Shape Groove”, Transactions of the JSME, Vol. C-66, No. 641, pp. 306-313, January 2000, (in Japanese with English abstract).
- [5] Waitz, I. A. et al, “Combustors for Micro-Gas turbine Engines”, Journal of Fluid Engineering, March 1998, Vol. 120, pp. 109-117.
- [6] Sugimoto, S., et al., Three-Dimensional Micromachining of Silicon Nitride for Power Microelectromechanical Systems, Digest of Technical Papers, Transducers’01, Eurosensors XV (The 11th International Conference on Solid-State Sensors and Actuators), Munich, Germany, June (2001) pp. 1140-1143.
- [7] Tanaka, S., et al., Silicon nitride ceramic-based 2-dimensional micro-combustor, J. Micromech. Microeng., 13 (2003) pp. 502-508.
- [8] Shuji Tanaka et al., Silicon Carbide Micro-reaction-sintering Using Micromachined Silicon Molds, J. Microelectromech. Syst., 10 (2001) pp. 55-61.

